# SPNS2 enables T cell egress from lymph nodes during an immune response

**Martyna Okuniewska**[1,5], **Victoria Fang**[1,3,5], **Audrey Baeyens**[1], **Varsha Raghavan**[1], **June-Yong Lee**[1,4], **Dan R. Littman**[1,2], **Susan R. Schwab**[1,6,*]

[1]Skirball Institute of Biomolecular Medicine, New York University Grossman School of Medicine, New York, NY 10016, USA

[2]Howard Hughes Medical Institute, New York, NY 10016, USA

[3]Present address: Department of Dermatology, University of Pennsylvania School of Medicine, Philadelphia, PA 19103, USA

[4]Present address: Department of Microbiology and Immunology, Yonsei University College of Medicine, Seoul, Korea

[5]These authors contributed equally

[6]Lead contact

## SUMMARY

T cell expression of sphingosine 1-phosphate (S1P) receptor 1 (S1PR1) enables T cell exit from lymph nodes (LNs) into lymph, while endothelial S1PR1 expression regulates vascular permeability. Drugs targeting S1PR1 treat autoimmune disease by trapping pathogenic T cells within LNs, but they have adverse cardiovascular side effects. In homeostasis, the transporter SPNS2 supplies lymph S1P and enables T cell exit, while the transporter MFSD2B supplies most blood S1P and supports vascular function. It is unknown whether SPNS2 remains necessary to supply lymph S1P during an immune response, or whether in inflammation other compensatory transporters are upregulated. Here, using a model of dermal inflammation, we demonstrate that SPNS2 supplies the S1P that guides T cells out of LNs with an ongoing immune response. Furthermore, deletion of *Spns2* is protective in a mouse model of multiple sclerosis. These results support the therapeutic potential of SPNS2 inhibitors to achieve spatially specific modulation of S1P signaling.

## In brief

Okuniewska et al. demonstrate that the transporter SPNS2 supplies the S1P that guides T cells out of lymph nodes with an ongoing immune response, and *Spns2* deletion is protective in a multiple sclerosis model. This highlights the therapeutic potential of SPNS2 inhibitors to achieve spatially specific modulation of S1P signaling.

## Graphical Abstract
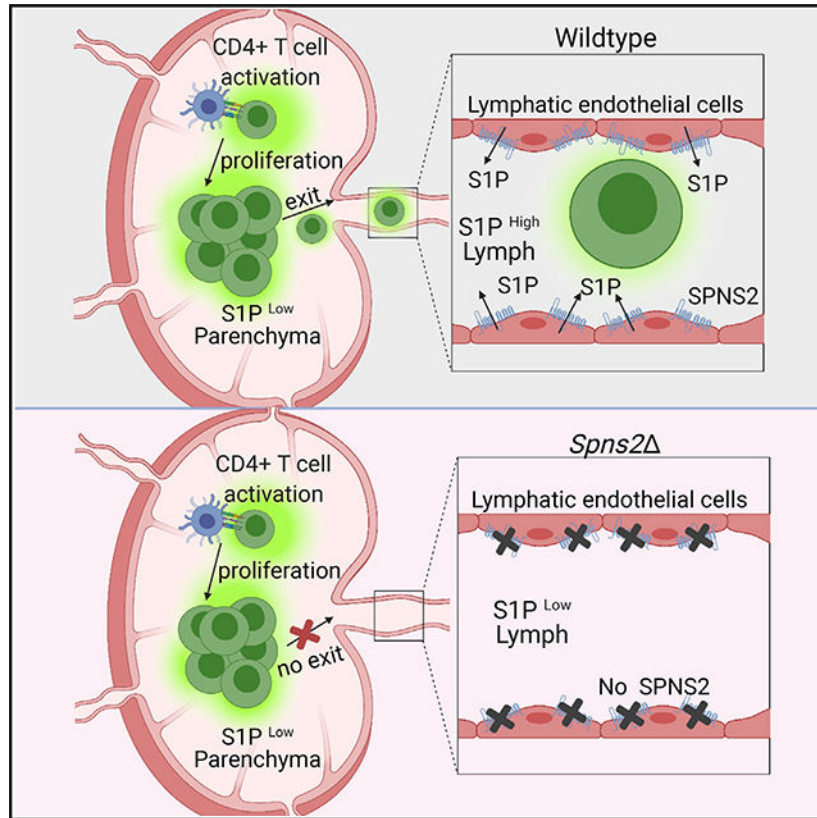


## INTRODUCTION

In the immune system, the most notable role of the signaling lipid sphingosine 1-phosphate (S1P) is to direct leukocyte exit from tissues, where the concentration of S1P is relatively low, into circulation, where the concentration of S1P is high (Baeyens and Schwab, 2020). Lymph S1P, produced by lymphatic endothelial cells, guides lymphocytes from lymph nodes (LNs) and Peyer's patches into lymph, while blood S1P, produced largely by red blood cells, enables exit from spleen into blood. T and B cells sense these S1P gradients primarily through the G protein-coupled receptor S1P receptor 1 (S1PR1). At least a dozen drugs targeting S1PR1 have entered clinical trials to treat autoimmune diseases, including multiple sclerosis, colitis, and psoriasis (Stepanovska and Huwiler, 2020). The first-in-class FTY720/fingolimod, as well as the next-generation therapeutics ozanimod, siponimod, and ponesimod, have received US Food and Drug Administration (FDA) approval for treatment of multiple sclerosis. These drugs are believed to work in large part by trapping pathogenic

T cells in LNs and preventing them from reaching the central nervous system (Brinkmann et al., 2010).

However, in the organism as a whole, the most notable role of S1P is in the cardiovascular system; mice that lack S1PR1 or both sphingosine kinases die at mid-gestation of hemorrhage (Liu et al., 2000; Mizugishi et al., 2005). S1P provided by red blood cells supports vascular development during embryogenesis and maintains endothelial junction integrity in adults (Camerer et al., 2009; Xiong et al., 2014). Macular edema is one side effect of FTY720, likely because chronic administration of FTY720 induces ubiquitination and degradation of endothelial S1PR1 (Camm et al., 2014). Cardiac arrhythmia is another important side effect of FTY720; this occurs primarily after administration of the first dose and is thought to be due to acute agonism of S1PR1 on cardiomyocytes prior to receptor degradation and desensitization (Camm et al., 2014). Thus, there is a need to develop therapeutics with greater specificity.

One strategy to achieve greater specificity is to manipulate S1P metabolism as opposed to S1PR1, and an attractive target is the step of S1P export. S1P is generated intracellularly by sphingosine kinases and must be exported from cells to signal to S1P receptors. We are only beginning to understand how cells transport S1P into the extracellular space. Spinster homolog 2 (SPNS2), a major facilitator superfamily transporter, was the first S1P transporter with measurable roles *in vivo* (Fukuhara et al., 2012; Hisano et al., 2012; Kawahara et al., 2009; Mendoza et al., 2012; Nagahashi et al., 2013; Nijnik et al., 2012). S1P levels in lymph are dramatically reduced in SPNS2-deficient mice, and this is due to a requirement for SPNS2 in lymphatic endothelial cells (Mendoza et al., 2012). In SPNS2-deficient mice, T cells cannot exit LNs into lymph, leading to a loss of circulating cells (Mendoza et al., 2012). By contrast, although SPNS2 contributes to supplying blood plasma S1P, it is not the major player (Fukuhara et al., 2012; Hisano et al., 2012; Mendoza et al., 2012; Nagahashi et al., 2013; Nijnik et al., 2012). Blood S1P levels remain at about 80% of baseline in SPNS2-deficient mice, and these mice have normal lung vascular permeability, unlike FTY720-treated animals (Mendoza et al., 2012; van der Weyden et al., 2017). Instead, blood S1P is supplied largely by red blood cells using a distinct major facilitator superfamily transporter, major facilitator superfamily domain containing protein 2B (MFSD2B) (Kobayashi et al., 2018; Pappu et al., 2007; Vu et al., 2017).

SPNS2 remains the only known protein required for lymph but not blood S1P, and we thus considered targeting SPNS2 as a strategy to trap autoreactive T cells in LNs while minimizing cardiovascular side effects. However, the studies of SPNS2's contribution to lymph S1P were carried out in homeostasis, and the role of SPNS2 in lymphocyte egress from LN in disease is poorly understood. A key outstanding question is whether other transporters are upregulated and compensate for the loss of SPNS2 during an immune response. In addition to MFSD2B, several ABC transporters have been reported to be necessary for S1P export by cultured cells (Lee et al., 2007; Mitra et al., 2006; Nieuwenhuis et al., 2009; Sato et al., 2007; Takabe et al., 2010). α9 integrin signaling in lymphatic endothelial cells promotes S1P secretion in inflammation, but not homeostasis, although the mechanism is not clear (Ito et al., 2014). Additionally, SPNS2 has been suggested as a target for cancer treatment, based on its role in metastasis (van der Weyden et al., 2017).

The existence of an additional S1P transporter that enables T cell exit from LN during an immune response might be important if cancer patients were treated with a SPNS2 inhibitor.

Here, using a well-defined model of inflammation, we demonstrate that SPNS2 is required to supply the S1P that guides effector T cells out of a LN with an ongoing immune response. Without SPNS2, T cell accumulation in inflamed tissue is substantially reduced. Furthermore, deletion of *Spns2* is protective in a murine model of multiple sclerosis, experimental autoimmune encephalitis, and this protection correlates with reduced T cell infiltration of the central nervous system. These results indicate that SPNS2 inhibitors may achieve spatially specific modulation of S1P signaling. They suggest the promise of SPNS2 inhibition for treatment of autoimmune disease but raise caution about this strategy in cancer.

## RESULTS AND DISCUSSION

### SPNS2 enables activated T cells to accumulate at a site of inflammation

We first asked whether SPNS2 is required for T cells to accumulate in an inflamed tissue using a well-defined model of dermal inflammation (McLachlan et al., 2009). In this model, OT-II TCR transgenic CD4$^+$ T cells (GFP$^+$ or CD45.1$^+$) were adoptively transferred to CD45.2$^+$ host mice. OT-II cells recognize the ovalbumin (OVA) peptide OVA$^{323-339}$ presented by A$^b$ (Barnden et al., 1998). One day later, one ear was injected with OVA emulsified in incomplete Freud's adjuvant (IFA). The other ear received a PBS control injection. Four days after IFA-OVA injection, ears were isolated to measure OT-II cell accumulation (Figure 1A). OT-II accumulation in inflamed ears was reduced 5-fold in SPNS2-deficient mice compared with littermate controls. The reduction was observed in mice lacking *Spns2* in lymphatic endothelial cells (*Spns2*$^{Lyve1}$; *Spns2*$^{f/f}$*Lyve1*-Cre) (Pham et al., 2010) and in mice with widespread tamoxifen-inducible deletion of *Spns2* (*Spns2*$^{UBC}$; *Spns2*$^{f/f}$*UBC*-CreERT2) (Ruzankina et al., 2007) (Figures 1B and 1C). The lack of OT-II cells in the ear of SPNS2-deficient mice did not simply reflect a lack of OT-II T cell proliferation in the draining LN (dLN), because there was no difference in OT-II cell numbers in the dLN (Figure 1D).

### SPNS2 enables activated T cells to access lymph

Having shown that SPNS2 is required for T cells to accumulate efficiently in a peripheral site of inflammation, we next asked whether the role of SPNS2 is to enable LN egress as hypothesized, or whether SPNS2 plays other roles, such as enabling T cell extravasation from blood into peripheral tissues. Because T cells exit LN into lymph, if exit were impaired in SPNS2-deficient mice, activated T cells should be found in LNs, but not lymph.

Lymph can be collected from the cisterna chyli, which drains lymph from the lower body. Thus, to quantify the number of activated OT-II cells in dLNs and lymph fluid, we modified the ear inflammation model and instead injected footpads with IFA-OVA. OT-II cells similarly did not accumulate efficiently within the foot tissue of *Spns2* mice compared with littermate controls (Figure 2A). dLNs of *Spns2* mice contained similar numbers of OT-II cells as littermate controls, again suggesting that SPNS2 deficiency does not substantially

affect the proliferation of antigen-specific cells (Figure 2B). However, fewer activated OT-II cells were in the lymph and blood of *Spns2* mice than controls (Figures 2C–2E), consistent with a LN exit defect.

## SPNS2 supplies lymph S1P during an immune response

We next sought to determine whether the loss of circulating T cells reflected the loss of an S1P gradient between the LN parenchyma and the lymph of an inflamed LN. We were unable to use our previously reported S1P reporter mouse (Fang et al., 2017; Ramos-Perez et al., 2015), because we did not detect enough reporting cells in cortical lymphatic sinuses, which are one of the primary sites of T cell egress from LNs (Benechet et al., 2016; Grigorova et al., 2009). Therefore, we developed an alternate method based on the finding that S1PR1 is internalized once bound to S1P, and hence the level of cell surface S1PR1 can be used to measure a cell's exposure to S1P (Liu et al., 1999; Schwab et al., 2005). We injected an allophycocyanin (APC)- or phycoerythrin (PE)-conjugated antibody to CD45 into inflamed footpads or ears 4 days after IFA-OVA injection and harvested dLNs 10 min later. In that time frame, the antibody drained into the dLNs and labeled cells within the subcapsular sinus and a subset of cortical and medullary lymphatic sinuses, but it did not substantially label parenchymal cells (Figures 3A and 3B) (Gerner et al., 2015). We measured S1PR1 levels on the surface of unlabeled T cells in the parenchyma and labeled T cells within (or probing) the lymphatic sinuses of the dLNs by flow cytometry (Figure 3C). We gated on CD44$^{lo}$CD69$^{-}$ naive CD4$^{+}$ T cells to avoid ligand-independent activation-induced regulation of surface S1PR1.

In inflamed LNs of control animals, as expected, T cells in lymph fluid (APC$^{+}$ or PE$^{+}$) had lower S1PR1 surface staining than T cells in the LN parenchyma (APC$^{-}$ or PE$^{-}$), reflecting the S1P gradient that guides T cells out of the LN. In inflamed LNs of SPNS2-deficient animals, T cells in the lymph had high S1PR1 staining compared with T cells in the lymph of controls, and there was no difference in S1PR1 surface staining on T cells in the lymph fluid compared with those in the parenchyma (Figures 3C and 3D). This demonstrated that even in inflammatory settings, SPNS2 is required to generate the high levels of lymph S1P required for T cell exit. Consistent with previous studies, S1PR1 levels on T cells in the LN parenchyma were roughly 5-fold higher in SPNS2-deficient mice compared with controls (Mendoza et al., 2012). This likely reflects lack of exposure to low levels of S1P in the LN parenchyma, as well as lack of periodic exposure to S1P in circulatory fluids (Fang et al., 2017).

## SPNS2-deficient mice are protected from experimental autoimmune encephalomyelitis (EAE)

Finally, we asked whether SPNS2 was required for pathology in a more clinically relevant model. FTY720, ozanimod, simponimod, and ponesimod, all of which target S1PR1, are FDA approved for treatment of multiple sclerosis. In multiple sclerosis, autoreactive T cells clonally expand, exit LN into lymph, circulate through blood, cross the blood-brain barrier, and cause demyelination and axonal damage in the brain (Brinkmann et al., 2010). Many of the currently FDA-approved drugs for multiple sclerosis, including drugs targeting S1PR1, were tested in murine experimental autoimmune encephalomyelitis (EAE) models

(Brinkmann et al., 2010). Multiple sclerosis patients receive drugs targeting S1PR1 when they reach remission to prevent a new wave of activated T cells from exiting LN and infiltrating the brain. This is modeled in mice by administering FTY720 before EAE induction (Brinkmann, 2009).

We predicted that if SPNS2 were required for activated T cell exit from LN, SPNS2 deficiency should ameliorate EAE. We treated adult *Spns2*$^{UBC}$ mice and littermate controls with five doses of tamoxifen to delete *Spns2* in a wide range of cells, and induced EAE 11 days later. *Spns2*$^{UBC}$ mice exhibited lower disease scores and reached endpoints less rapidly than control animals (Figures 4A–4C). This protection correlated with a reduction of the number of activated T cells in the central nervous system (Figure 4D; Figures S1 and S2). These results suggested that SPNS2 inhibition may be effective in treatment of tissue inflammatory diseases. Consistent with our results, *Spns2*$^{-/-}$ mice are also protected from EAE (Donoviel et al., 2015). However, it had been unclear to what extent this protection resulted from defects caused by *Spns2* deficiency throughout development, including a substantial loss of naive T cells (Fukuhara et al., 2012; Hisano et al., 2012; Mendoza et al., 2012; Nagahashi et al., 2013; Nijnik et al., 2012). Deletion of *Spns2* just prior to EAE induction more closely mimics drug treatment of patients in remission.

Here we validated a method for measuring S1P gradients between the parenchyma and lymphatic sinuses within a single LN. We found that SPNS2 generates the S1P gradient that directs T cell exit from LN into lymph during an immune response, and that deleting *Spns2* just prior to EAE induction protects mice from disease. Our results provide rationale and mechanistic insight for developing SPNS2 inhibitors for clinical use in autoimmune diseases. Inhibition of SPNS2 has also been suggested to have potential in treating cancer, because deletion of *Spns2* protects against seeding of melanoma tumor cells in the lung after intravenous injection (van der Weyden et al., 2017). Our work suggests that treating tumors with a SPNS2 inhibitor may also trap effector T cells within LNs and prevent them from accessing tumor tissue. The balance and mechanisms of these effects of SPNS2 inhibition in disease will be essential to understand as new therapeutics are developed.

## STAR★METHODS

### RESOURCE AVAILABILITY

**Lead contact—**Further information and requests for resources and reagents should be directed to and will be fulfilled by the Lead Contact, Susan Schwab, Susan.Schwab@med.nyu.edu.

**Materials availability—**This study did not generate new unique reagents.

**Data and code availability—**Source data are available at https://doi.org/10.17632/2wkphfrn84.2.

### EXPERIMENTAL MODEL AND SUBJECT DETAILS

**Mice—***Spns2*$^{f/f}$ (Mendoza et al., 2012), *Lyve1*-Cre (Pham et al., 2010), *UBC*-CreERT2 (Ruzankina et al., 2007), *UBC*-GFP (Schaefer et al., 2001), and OT-II mice (Barnden et

al., 1998) have been described. C57BL/6 and CD45.1$^+$ C57BL/6 congenic mice were from Charles River Laboratories or Jackson Laboratories. All mice were on a C57BL/6 or a mixed B6–129 background. Mice were used at 6–40 weeks of age. Female and male mice were used depending on availability, except for EAE experiments, which used females. For induction of *UBC*-CreERT2, adult mice received daily intraperitoneal (i.p.) injections of 200 μg tamoxifen for 5 d, and were analyzed at least 5 d after the final tamoxifen dose (all mice in each litter, with and without Cre, were treated with tamoxifen). Mice were housed in specific pathogen–free conditions at the Skirball Institute Animal Facility. All cages were on a 12:12-h light:dark cycle (lights on, 0700) in a temperature- and humidity-controlled room. Room temperature was maintained at $72 \pm 2°F$ ($22.2 \pm 1.1°C$), and room humidity was maintained at 30% to 70%. All animal experiments were performed in accordance with protocols approved by the New York University Institutional Animal Care and Use Committee.

Littermates (when possible of the same sex) were randomly allocated to experimental groups. No animals were excluded unless they were clearly sick (hunched, low body weight) prior to EAE induction. These criteria were pre-established, and are standard in the laboratory. All EAE scoring was blinded. For unblinded experiments, the order of sample collection and data acquisition was designed to avoid experimental bias: collection and processing of samples from control and knockout animals were alternated.

## METHOD DETAILS

**OVA-IFA model**—Lymphocytes were isolated from spleen and LN of OT-II TCR Tg GFP$^+$ mice or OT-II TCR Tg CD45.1$^+$ mice, and in some cases labeled with CellTrace Violet Cell Proliferation Kit (ThermoFisher C34557, according to the manufacturer's instructions). $1 \times 10^6$ OT-II T cells (Vβ5$^+$CD4$^+$) were transferred into recipient mice by tail vein injection in 200μl. A 10μl emulsion of 1:1 IFA and 25μg OVA (Sigma A2512) in PBS was injected into ears (i.d.) or footpads (s.c.) 1 day after T cell transfer. When indicated, mice were treated with FTY720 at a dose of 1 mg per kg body weight i.p. daily starting on the day of or the day after immunization with IFA-OVA. FTY720 (Cayman Chemical) was resuspended at 100 μg/ml in 2% beta-hydroxylpropyl-cyclodextrin in PBS. Animals were euthanized 4 d after IFA-OVA injection.

**Anti-CD45 injection**—Mice were injected i.d. in the ear (10μl) or s.c. in the footpad (20μl) with PE- or APC-conjugated antibody to CD45.2 (clone 104, 0.2μg). Animals were euthanized 10 minutes later, and dLN were collected.

**EAE induction**—To induce EAE, a 1:1 incomplete Freund's adjuvant (IFA) to PBS emulsion was prepared with final concentrations of 2 mg/ml desiccated Mycobacterium tuberculosis (Difco 231141) (to make complete Freund's adjuvant, CFA) and 0.5 mg/ml myelin oligodendrocyte (MOG) peptide 35–55 (Genscript RP10245). Three injections were administered s.c. in the back skin (100 μl per site) such that each mouse received 150 μg total MOG. At the time of MOG immunization and 1 d later, 200 ng pertussis toxin (List Biological 181) was injected i.p. Mice were weighed and scored on alternating days or daily, depending on disease score. Animals were scored for clinical symptoms as follows: 0, no

signs of disease; 1, decreased tail tone or flaccid tail; 2, weakness in the limbs and loss of righting reflex; 3, inability to move one or both hindlimbs, and urinary incontinence; 4, weakness of both forelimbs and hindlimbs, complete hindlimb paralysis, and atonic bladder; 5, moribund. Any mouse that reached a score of 4 for more than 24h or that reached a score of 5 was euthanized.

Midway through the work, the *Spns2* colony was rederived at Jackson Laboratory (as part of the reorganization of NYU's mouse housing after Hurricane Sandy). Afterward, EAE induction was highly variable. To standardize this, we colonized all mice used in experiments with segmented filamentous bacteria (SFB). Fecal pellets were collected from live SFB-monoassociated mice and frozen at −80° until use. Frozen feces were homogenized and filtered through a 100 μm cell strainer. Two fecal pellets were resuspended per 1 mL sterile PBS and supernatants were introduced into mice (200 μl/animal) by oral gavage for two consecutive days.

Fecal pellets were collected from mice pre- and 1 week post- oral SFB gavage. SFB colonization was confirmed by qPCR. Phenol-chloroform DNA extraction was performed on frozen fecal pellets that were weighed prior to DNA extraction. Individual fecal pellets were placed in 2 mL polypropylene tubes together with 0.5 mL of 0.1 mm zirconia/silica beads (BioSpec 11079101z), 500 μL of DNA extraction buffer (200mM Tris pH 8.0, 200mM NaCl, and 20mM EDTA), 200 μL of 20% SDS, and 500 μL of phenol:chloroform:isoamyl alcohol (25:24:1). Bacterial cells in the sample were lysed using a bead-beater (Retsch MM301) for 5 minutes at maximum speed. After lysis, the samples were centrifuged at 16,000 g for 5 minutes at 4°C and the DNA-containing aqueous phase was collected and subjected to one additional extraction with 500 μL of DNA extraction buffer to further remove contaminants. DNA was precipitated with 35 μl 3M sodium acetate pH 5.5 (Invitrogen AM9740) and 770 μl 100% ethanol at −80°C for 10–20 minutes followed by centrifugation for 20 minutes at 16,000 g at 4°C. After washing in 70% ethanol, the DNA pellet was dried and resuspended in nuclease free water.

qPCR was conducted on the fecal DNA to determine the amount of SFB and total bacterial load in each sample by amplifying 16S rRNA genes using the following SFB-specific primers (Barman et al., 2008) 5′-GACGCTGAGGCATGAGAGCAT-3′ and 5′-GACGGCACGGATTGTTATTCA-3′, and universal primers 5′- ACTCCTACGGGAGGCAGCAGT-3′ and 5′-ATTACCGCGGCTGCTGGC-3′ for 16S rRNA (Amann et al., 1990). qPCR was performed with the SYBR GREEN I Master Mix (Roche 04707516001) on the Roche Lightcycler 480 according to the manufacturer's instructions, with the following cycle conditions: 90°C for 5 min, then 40 cycles of 95°C for 10 s, 60°C for 30 s, and 72°C for 30 s. Colonization was considered successful when more SFB was found in the fecal pellets post-gavage as compared to pre-gavage in the same mice. On average, pre-gavage Ct values for the SFB primers were 28 cycles and post-gavage Ct values were 23 cycles, while average Ct values for the universal primers were 17.5 cycles.

**Confocal microscopy—**LN were isolated, fixed in 4% PFA for 1 h at 22–25°C with gentle shaking, dehydrated by sucrose gradient (15% sucrose in PBS > 1h at 4°C, then 30%

sucrose at 4°C overnight), embedded in OCT (Sakura), and snap-frozen in dry ice-cooled 2-methylbutane. 8- to 12-μm sections were cut and air-dried. All staining was performed at 22–25°C. Sections were permeabilized for 10–30 min with 0.5% Triton X-100 in PBS, then incubated for 10–30 min in block buffer consisting of 0.1% Triton X-100 in PBS with 4% normal rat serum, 4% normal mouse serum, and 10 μg/ml anti-CD16/32 (BioLegend, clone 93). Stains were done with antibodies diluted in the block buffer. Slides were mounted with Fluoromount-G (Southern Biotech) and visualized using a Zeiss 710 inverted confocal microscope with a 25 × or 40 × oil-immersion objective and ZEN 2010 software. Image analysis was done with ImageJ software v1.49 (NIH).

**Isolation and restimulation of cells from the brain and spinal cord—**Mice were euthanized by CO2 inhalation and perfused with 20mL ice-cold 5mM EDTA in PBS. Brain and spinal cord were isolated and minced (separately) with scissors in 2mL digestion buffer (HBSS + 10% FBS supplemented with 20mM HEPES, 100 IU/ml penicillin, 100μg/ml streptomycin). Collagenase D (Sigma Aldrich 11088866001) was added to a final concentration of 0.5mg/mL, and the tissue was incubated at 37°C for 35 minutes in a 6 well plate. 5 μL of 0.5M EDTA was added for 5 minutes at 37°C to stop the reaction. Samples were passed through a 18G needle with 10mL of additional HBSS + 10% FBS to achieve a single cell suspension. The suspension was filtered through a 70 μm cell strainer into a 15mL conical tube and spun at 1500rpm for 10 minutes at 4°C. The pellet was resuspended in 7mL of 35% Percoll in digestion buffer (for 100 mL: 3.8 mL 10X PBS, 34.2 mL Percoll, 62 mL digestion buffer) and centrifuged at 2000 rpm at room temperature with no brake for 30 minutes. The cells were resuspended in digestion buffer and spun at 400 g for 4 minutes at 4C. The pellet was resuspended in 400 μl PBS+ 2% FBS and split into two samples, one of which was used for flow cytometry and the other used for restimulation followed by flow cytometry. For restimulation of cells for IL-17A and IFN-γ staining, cells were stimulated for 3 hours at 37°C with PMA (50 ng/ml) (Sigma P8139) and ionomycin (420ug/ml) (Sigma I9657) in RPMI 1640 medium containing HEPES (10 mM), penicillin (100 IU/ml), streptomycin (100 μg/ml), β-mercaptoethanol (50 μM), 10% FBS and 1 μl/ml of GolgiPlug (BD Biosciences 555029). Cells were then washed in PBS with 2% FBS, and were subsequently stained for flow cytometry.

**Isolation of cells from lymphoid organs and skin—**Lymphocytes were isolated from spleen and LN by mechanical disruption and filtration through a 70 μm cell strainer. Lymphocytes from ears and footpads were isolated as previously described (Naik et al., 2012). Briefly, ears were separated into ventral and dorsal halves with forceps, and footpads were minced with scissors. Tissues were incubated for 2h at 37°C in 750μl skin digestion media consisting of 0.25mg/ml Liberase TL (Roche 05401020001) and 0.25mg/ml DNase I (Sigma DN25) in RPMI1640 supplemented with 100 U/ml penicillin, 100μg/ml streptomycin, 55 mM β-mercaptoethanol, and 20mM HEPES. Skin digestion media was then inactivated with 750μl ice-cold RPMI 1640 supplemented as above and containing 3% FBS and 15μl of 0.5M EDTA. Digested tissues were processed using the Medicon (BD 340592)/Medimachine tissue homogenizer system (BD 340588) for 4 minutes. The Medicon was washed with an additional 8.5ml of RPMI1640 supplemented as above and containing 10% FBS (no EDTA), and the media containing cells was passed through a 50

μm syringe Filcon cell strainer (BD 340603). Lymphocytes were enumerated with a cell counter (Beckman Coulter Multisizer 3) set to detect nuclei between 3.5 and 10 μm.

**Cell staining and flow cytometry**—For intracellular staining, cells were fixed and permeabilized with the Transcription-Factor Buffer Set (BD PharMingen 562574) according to the manufacturer's instructions and subsequently stained for FoxP3 or for IL17A and IFN-γ for 45 minutes at room temperature.

Staining for S1PR1 was done on ice in PBS supplemented with 0.05% sodium azide, 1 mM EDTA and 0.5% FBS. Cells were stained for 90 min with anti-mouse S1PR1 (7.2 μg/ml; MAB7089, R&D Systems), washed twice in buffer, stained for 45 min with anti-rat IgG-biotin F(ab′)2 (9.5 μg/ml; 2340649, Jackson Immunoresearch), washed twice in buffer, and stained with streptavidin coupled with APC or PE-Cy7 and the other surface membrane antibodies.

Cells were analyzed on an LSRII (BD). Data were analyzed with FlowJo software Version 10 (TreeStar).

**Antibodies**—The following fluorochrome-conjugated antibodies and reagents were used: anti-CD3 (145–2C11, 5 μg/ml for flow cytometry and 10μg/ml for microscopy), anti-CD4 (RMA 4–5, 1 μg/ml), anti-CD8 (53–6.7, 2.5 μg/ml), anti-CD44 (IM7, 2.5μg/ml), anti-B220/CD45RO (RA3–6B2, 2.5 μg/ml), anti-CD69 (H1.2F3, 2μg/ml), anti-NK1.1 (PK136, 0.5 mg/ml), anti-I-A/I-E (M5/114.15.2, 0.2 mg/ml), anti-CD11c (N418, 0.2 mg/ml), anti-CD14 (Sa14–2, 0.2 mg/ml), anti-CD45.1 (A20, 0.5 mg/ml), anti-CD45.2 (104, 0.5 mg/ml), anti-IL-17A (TC11–18H10.1, 0.2 mg/ml), anti-IFN-γ (XMG1.2, 0.2 mg/ml), streptavidin (2.5 μg/ml for flow cytometry and 1.25μg/ml for microscopy) (all from BioLegend). Fluorochrome-conjugated anti-Lyve1 (ALY7, 2.5 μg/ml), anti-FoxP3 (FJK-16 s, 0.5 mg/ml) were from eBioscience. Anti-S1PR1 (clone 713412) was from R&D Systems. CD4 (RMA 4–5, 0.2 mg/ml) was from BD Biosciences. Propidium iodide (0.75μg/ml), DAPI (0.125μg/ml) or LIVE/DEAD Fixable Blue Dead Cell Stain (ThermoFisher L23105) was used to exclude dead cells.

## QUANTIFICATION AND STATISTICAL ANALYSIS

Statistical analysis was performed using GraphPad Prism v.9. Samples were compared by Student′s two-tailed unpaired t test. In comparing disease scores in the EAE model, genotypes were compared by Student's two-tailed unpaired t test corrected for multiple comparisons by the Holm-Sidak method. Survival differences were compared by a Log-rank Mantel-Cox test.

## Supplementary Material

Refer to Web version on PubMed Central for supplementary material.

## ACKNOWLEDGMENTS

## REFERENCES

Amann RI, Binder BJ, Olson RJ, Chisholm SW, Devereux R, and Stahl DA (1990). Combination of 16S rRNA-targeted oligonucleotide probes with flow cytometry for analyzing mixed microbial populations. Appl. Environ. Microbiol. 56, 1919–1925. [PubMed: 2200342]

Baeyens AAL, and Schwab SR (2020). Finding a Way Out: S1P Signaling and Immune Cell Migration. Annu. Rev. Immunol. 38, 759–784. [PubMed: 32340572]

Barman M, Unold D, Shifley K, Amir E, Hung K, Bos N, and Salzman N (2008). Enteric salmonellosis disrupts the microbial ecology of the murine gastrointestinal tract. Infect. Immun. 76, 907–915. [PubMed: 18160481]

Barnden MJ, Allison J, Heath WR, and Carbone FR (1998). Defective TCR expression in transgenic mice constructed using cDNA-based alpha- and beta-chain genes under the control of heterologous regulatory elements. Immunol. Cell Biol. 76, 34–40. [PubMed: 9553774]

Benechet AP, Menon M, Xu D, Samji T, Maher L, Murooka TT, Mempel TR, Sheridan BS, Lemoine FM, and Khanna KM (2016). T cell-intrinsic S1PR1 regulates endogenous effector T-cell egress dynamics from lymph nodes during infection. Proc. Natl. Acad. Sci. USA 113, 2182–2187. [PubMed: 26862175]

Brinkmann V (2009). FTY720 (fingolimod) in Multiple Sclerosis: therapeutic effects in the immune and the central nervous system. Br. J. Pharmacol. 158, 1173–1182. [PubMed: 19814729]

Brinkmann V, Billich A, Baumruker T, Heining P, Schmouder R, Francis G, Aradhye S, and Burtin P (2010). Fingolimod (FTY720): discovery and development of an oral drug to treat multiple sclerosis. Nat. Rev. Drug Discov. 9, 883–897. [PubMed: 21031003]

Camerer E, Regard JB, Cornelissen I, Srinivasan Y, Duong DN, Palmer D, Pham TH, Wong JS, Pappu R, and Coughlin SR (2009). Sphingosine-1-phosphate in the plasma compartment regulates basal and inflammation-induced vascular leak in mice. J. Clin. Invest. 119, 1871–1879. [PubMed: 19603543]

Camm J, Hla T, Bakshi R, and Brinkmann V (2014). Cardiac and vascular effects of fingolimod: mechanistic basis and clinical implications. Am. Heart J. 168, 632–644. [PubMed: 25440790]

Donoviel MS, Hait NC, Ramachandran S, Maceyka M, Takabe K, Milstien S, Oravecz T, and Spiegel S (2015). Spinster 2, a sphingosine-1-phosphate transporter, plays a critical role in inflammatory and autoimmune diseases. FASEB J. 29, 5018–5028. [PubMed: 26324848]

Fang V, Chaluvadi VS, Ramos-Perez WD, Mendoza A, Baeyens A, Rivera R, Chun J, Cammer M, and Schwab SR (2017). Gradients of the signaling lipid S1P in lymph nodes position natural killer cells and regulate their interferon-γ response. Nat. Immunol. 18, 15–25. [PubMed: 27841869]

Fukuhara S, Simmons S, Kawamura S, Inoue A, Orba Y, Tokudome T, Sunden Y, Arai Y, Moriwaki K, Ishida J, et al. (2012). The sphingosine-1-phosphate transporter Spns2 expressed on endothelial cells regulates lymphocyte trafficking in mice. J. Clin. Invest. 122, 1416–1426. [PubMed: 22406534]

Gerner MY, Torabi-Parizi P, and Germain RN (2015). Strategically localized dendritic cells promote rapid T cell responses to lymph-borne particulate antigens. Immunity 42, 172–185. [PubMed: 25607462]

Grigorova IL, Schwab SR, Phan TG, Pham TH, Okada T, and Cyster JG (2009). Cortical sinus probing, S1P1-dependent entry and flow-based capture of egressing T cells. Nat. Immunol. 10, 58–65. [PubMed: 19060900]

Hisano Y, Kobayashi N, Yamaguchi A, and Nishi T (2012). Mouse SPNS2 functions as a sphingosine-1-phosphate transporter in vascular endothelial cells. PLoS ONE 7, e38941. [PubMed: 22723910]

Ito K, Morimoto J, Kihara A, Matsui Y, Kurotaki D, Kanayama M, Simmons S, Ishii M, Sheppard D, Takaoka A, and Uede T (2014). Integrin α9 on lymphatic endothelial cells regulates lymphocyte egress. Proc. Natl. Acad. Sci. USA 111, 3080–3085. [PubMed: 24516133]

Kawahara A, Nishi T, Hisano Y, Fukui H, Yamaguchi A, and Mochizuki N (2009). The sphingolipid transporter spns2 functions in migration of zebrafish myocardial precursors. Science 323, 524–527. [PubMed: 19074308]

Kobayashi N, Kawasaki-Nishi S, Otsuka M, Hisano Y, Yamaguchi A, and Nishi T (2018). MFSD2B is a sphingosine 1-phosphate transporter in erythroid cells. Sci. Rep. 8, 4969. [PubMed: 29563527]

Lee YM, Venkataraman K, Hwang SI, Han DK, and Hla T (2007). A novel method to quantify sphingosine 1-phosphate by immobilized metal affinity chromatography (IMAC). Prostaglandins Other Lipid Mediat. 84, 154–162. [PubMed: 17991617]

Liu CH, Thangada S, Lee MJ, Van Brocklyn JR, Spiegel S, and Hla T (1999). Ligand-induced trafficking of the sphingosine-1-phosphate receptor EDG-1. Mol. Biol. Cell 10, 1179–1190. [PubMed: 10198065]

Liu Y, Wada R, Yamashita T, Mi Y, Deng CX, Hobson JP, Rosenfeldt HM, Nava VE, Chae SS, Lee MJ, et al. (2000). Edg-1, the G protein-coupled receptor for sphingosine-1-phosphate, is essential for vascular maturation. J. Clin. Invest. 106, 951–961. [PubMed: 11032855]

McLachlan JB, Catron DM, Moon JJ, and Jenkins MK (2009). Dendritic cell antigen presentation drives simultaneous cytokine production by effector and regulatory T cells in inflamed skin. Immunity 30, 277–288. [PubMed: 19200757]

Mendoza A, Bréart B, Ramos-Perez WD, Pitt LA, Gobert M, Sunkara M, Lafaille JJ, Morris AJ, and Schwab SR (2012). The transporter Spns2 is required for secretion of lymph but not plasma sphingosine-1-phosphate. Cell Rep. 2, 1104–1110. [PubMed: 23103166]

Mitra P, Oskeritzian CA, Payne SG, Beaven MA, Milstien S, and Spiegel S (2006). Role of ABCC1 in export of sphingosine-1-phosphate from mast cells. Proc. Natl. Acad. Sci. USA 103, 16394–16399. [PubMed: 17050692]

Mizugishi K, Yamashita T, Olivera A, Miller GF, Spiegel S, and Proia RL (2005). Essential role for sphingosine kinases in neural and vascular development. Mol. Cell. Biol. 25, 11113–11121. [PubMed: 16314531]

Nagahashi M, Kim EY, Yamada A, Ramachandran S, Allegood JC, Hait NC, Maceyka M, Milstien S, Takabe K, and Spiegel S (2013). Spns2, a transporter of phosphorylated sphingoid bases, regulates their blood and lymph levels, and the lymphatic network. FASEB J. 27, 1001–1011. [PubMed: 23180825]

Naik S, Bouladoux N, Wilhelm C, Molloy MJ, Salcedo R, Kastenmuller W, Deming C, Quinones M, Koo L, Conlan S, et al. (2012). Compartmentalized control of skin immunity by resident commensals. Science 337, 1115–1119. [PubMed: 22837383]

Nieuwenhuis B, Lüth A, Chun J, Huwiler A, Pfeilschifter J, Schäfer-Korting M, and Kleuser B (2009). Involvement of the ABC-transporter ABCC1 and the sphingosine 1-phosphate receptor subtype S1P(3) in the cytoprotection of human fibroblasts by the glucocorticoid dexamethasone. J. Mol. Med. (Berl.) 87, 645–657. [PubMed: 19370318]

Nijnik A, Clare S, Hale C, Chen J, Raisen C, Mottram L, Lucas M, Estabel J, Ryder E, Adissu H, et al.; Sanger Mouse Genetics Project (2012). The role of sphingosine-1-phosphate transporter Spns2 in immune system function. J. Immunol. 189, 102–111. [PubMed: 22664872]

Pappu R, Schwab SR, Cornelissen I, Pereira JP, Regard JB, Xu Y, Camerer E, Zheng YW, Huang Y, Cyster JG, and Coughlin SR (2007). Promotion of lymphocyte egress into blood and lymph by distinct sources of sphingosine-1-phosphate. Science 316, 295–298. [PubMed: 17363629]

Pham TH, Baluk P, Xu Y, Grigorova I, Bankovich AJ, Pappu R, Coughlin SR, McDonald DM, Schwab SR, and Cyster JG (2010). Lymphatic endothelial cell sphingosine kinase activity is required for lymphocyte egress and lymphatic patterning. J. Exp. Med. 207, 17–27. [PubMed: 20026661]

Ramos-Perez WD, Fang V, Escalante-Alcalde D, Cammer M, and Schwab SR (2015). A map of the distribution of sphingosine 1-phosphate in the spleen. Nat. Immunol. 16, 1245–1252. [PubMed: 26502404]

Ruzankina Y, Pinzon-Guzman C, Asare A, Ong T, Pontano L, Cotsarelis G, Zediak VP, Velez M, Bhandoola A, and Brown EJ (2007). Deletion of the developmentally essential gene ATR in adult

mice leads to age-related phenotypes and stem cell loss. Cell Stem Cell 1, 113–126. [PubMed: 18371340]

Sato K, Malchinkhuu E, Horiuchi Y, Mogi C, Tomura H, Tosaka M, Yoshimoto Y, Kuwabara A, and Okajima F (2007). Critical role of ABCA1 transporter in sphingosine 1-phosphate release from astrocytes. J. Neurochem. 103, 2610–2619. [PubMed: 17931360]

Schaefer BC, Schaefer ML, Kappler JW, Marrack P, and Kedl RM (2001). Observation of antigen-dependent CD8+ T-cell/ dendritic cell interactions in vivo. Cell. Immunol. 214, 110–122. [PubMed: 12088410]

Schwab SR, Pereira JP, Matloubian M, Xu Y, Huang Y, and Cyster JG (2005). Lymphocyte sequestration through S1P lyase inhibition and disruption of S1P gradients. Science 309, 1735–1739. [PubMed: 16151014]

Stepanovska B, and Huwiler A (2020). Targeting the S1P receptor signaling pathways as a promising approach for treatment of autoimmune and inflammatory diseases. Pharmacol. Res. 154, 104170. [PubMed: 30776422]

Takabe K, Kim RH, Allegood JC, Mitra P, Ramachandran S, Nagahashi M, Harikumar KB, Hait NC, Milstien S, and Spiegel S (2010). Estradiol induces export of sphingosine 1-phosphate from breast cancer cells via ABCC1 and ABCG2. J. Biol. Chem. 285, 10477–10486. [PubMed: 20110355]

van der Weyden L, Arends MJ, Campbell AD, Bald T, Wardle-Jones H, Griggs N, Velasco-Herrera MD, Tüting T, Sansom OJ, Karp NA, et al.; Sanger Mouse Genetics Project (2017). Genome-wide in vivo screen identifies novel host regulators of metastatic colonization. Nature 541, 233–236. [PubMed: 28052056]

Vu TM, Ishizu AN, Foo JC, Toh XR, Zhang F, Whee DM, Torta F, Cazenave-Gassiot A, Matsumura T, Kim S, et al. (2017). Mfsd2b is essential for the sphingosine-1-phosphate export in erythrocytes and platelets. Nature 550, 524–528. [PubMed: 29045386]

Xiong Y, Yang P, Proia RL, and Hla T (2014). Erythrocyte-derived sphingosine 1-phosphate is essential for vascular development. J. Clin. Invest. 124, 4823–4828. [PubMed: 25250575]

## Highlights

- The S1P transporter SPNS2 enables effector T cells to accumulate in inflamed tissue

- SPNS2 generates the S1P gradient between LNs and lymph during an immune response

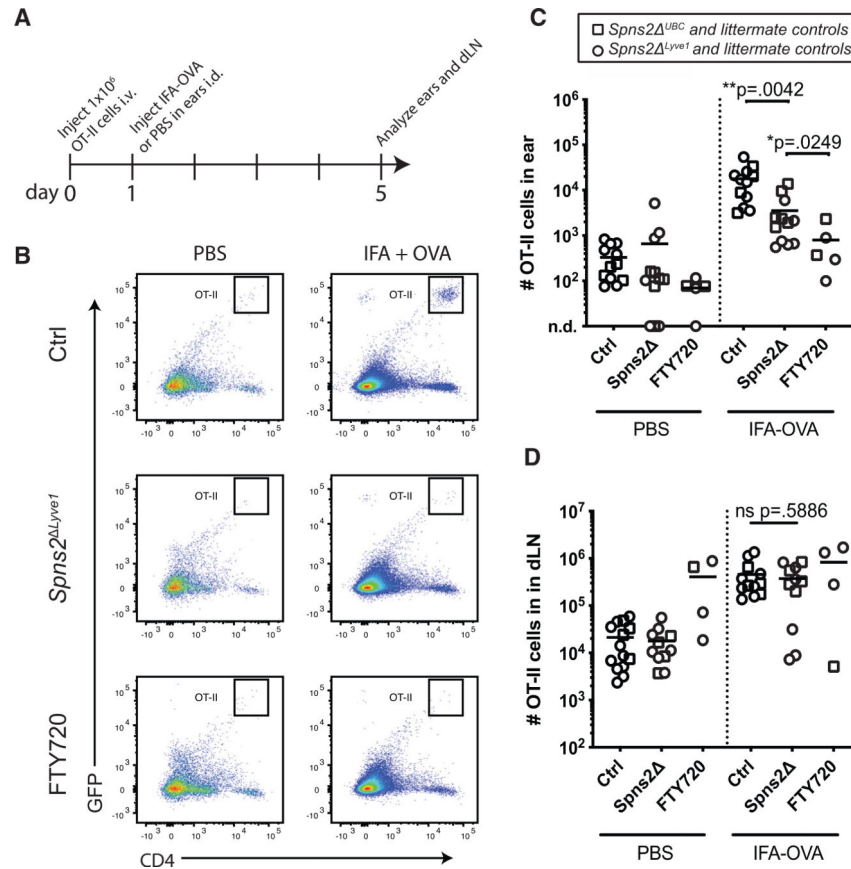- Loss of SPNS2 is protective in experimental autoimmune encephalomyelitis

**Figure 1. SPNS2 enables activated T cells to accumulate at a site of inflammation**

(A) Experiment schematic. OT-II T cells (GFP+ or CD45.1+) were adoptively transferred intravenously (i.v.) to CD45.2+ host mice. One day later, ears were injected intradermally (i.d.) with OVA-IFA or PBS (or untreated). Tissues were analyzed 4 days later.

(B) Representative flow cytometry plots showing transferred OT-II cells as GFP+ CD4+ cells in ears 4 days after i.d. injection with either IFA-OVA or PBS in *Spns2* $^{Lyve1}$ mice, littermate controls, and controls treated with FTY720. Plots are gated on CD45+ cells.

(C and D) Number of transferred OT-II cells in ears or cervical dLNs of ears with the indicated treatment. Each symbol represents an individual ear or dLN; bars indicate the mean. Squares indicate *Spns2* $^{UBC}$ mice or their littermate controls; circles indicate *Spns2* $^{Lyve1}$ mice or their littermate controls (FTY720 experiments used littermate controls of the indicated genotypes). Data are pooled from six (C) or seven (D) experiments. The FTY720 comparison was included in three experiments. Each experiment includes at least one littermate pair of SPNS2-deficient and control animals; some experiments had an odd number of animals if there were, for example, two SPNS2-deficient and one control animal in the litter. Statistics, two-tailed unpaired Student's t test.
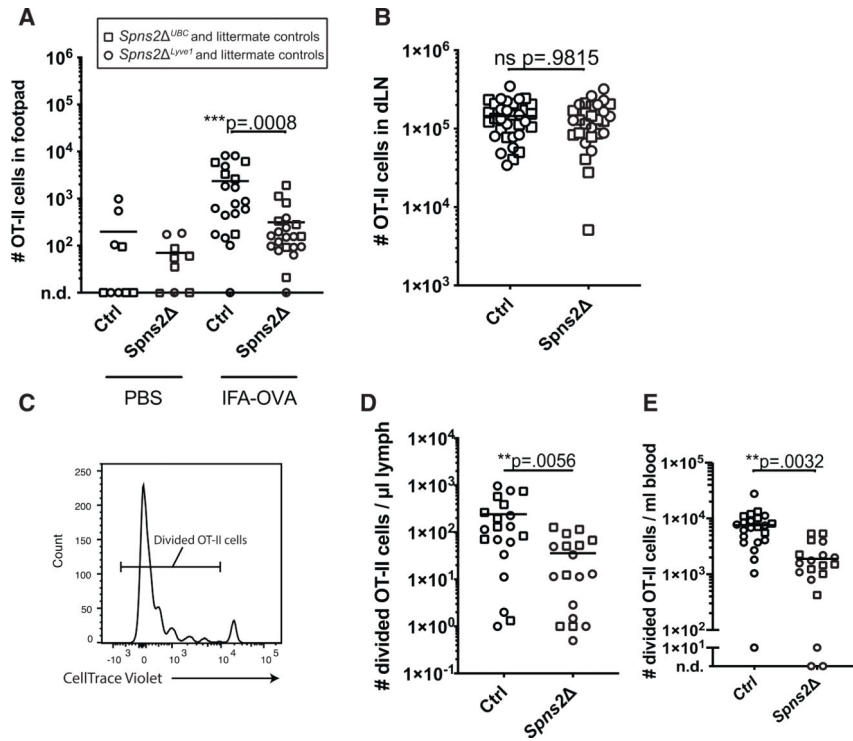
**Figure 2. SPNS2 enables activated T cells to access lymph**

(A and B) OT-II TCR transgenic CD4$^+$ T cells (GFP$^+$) labeled with CellTrace Violet (CTV) were adoptively transferred i.v. to host mice. One day later, footpads were subcutaneously (s.c.) injected with IFA-OVA or with PBS control. OT-II cells (GFP$^+$ CD4$^+$) were quantified 4 days later in footpads (A) or popliteal draining LNs (dLNs) (B). (B) The animals shown in (A) are compiled, as well as additional animals in which both footpads were injected with IFA-OVA. Each point is one dLN of a footpad injected with IFA-OVA.

(C–E) As in (A) and (B), and both footpads were injected with IFA-OVA. (C) Divided OT-II cells were defined using CTV dilution as shown. Representative histogram of OT-II cells from draining popliteal LNs. (D) Divided OT-II cell numbers in lymph. (E) Divided OT-II cell numbers in blood.

Each symbol represents an individual footpad (A), dLN (B), or mouse (D and E); bars indicate the mean. Squares indicate *Spns2*$^{UBC}$ mice or their littermate controls; circles indicate *Spns2*$^{Lyve1}$ mice or their littermate controls. Data are pooled from 7 (A), 11 (B and E), or 9 (D) experiments. Each experiment includes at least one littermate pair of SPNS2-deficient and control animals; some experiments had an odd number of animals if there were, for example, two SPNS2-deficient and one control animal in the litter. Statistics, two-tailed unpaired Student's t test.
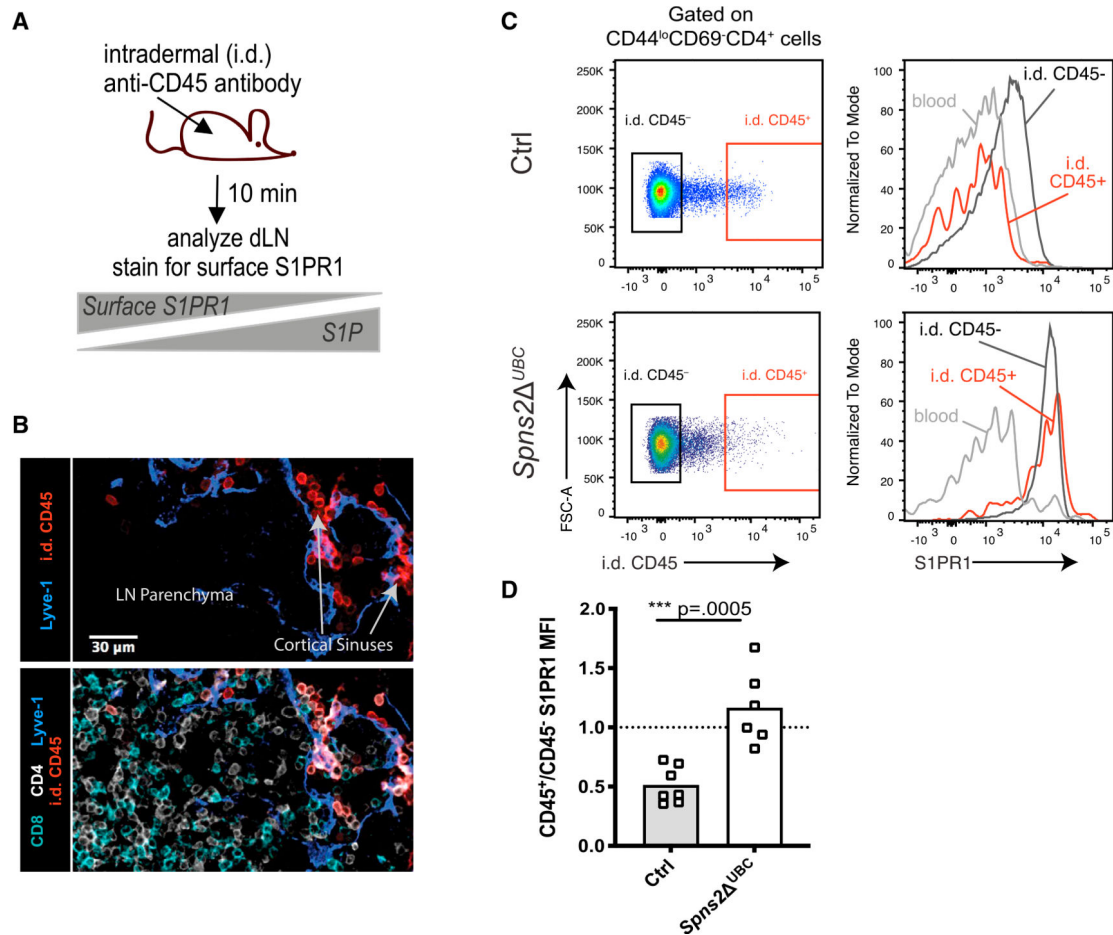
**Figure 3. SPNS2 supplies lymph S1P during an immune response**

(A) Experiment design. $Spns2^{UBC}$ and littermate control mice received $1 \times 10^6$ OT-II cells i.v. 1 day prior to IFA-OVA injection in ears and/or footpads. Four days after IFA-OVA injection, mice were injected with PE- or APC-conjugated anti-CD45 in the ear (i.d.) and/or footpad (s.c.). Mice were euthanized 10 min later, and dLNs were analyzed.

(B) dLNs were analyzed by confocal microscopy. Anti-CD45-labeled cells are found in lymph vessels, including cortical sinuses. Scale bar, 30 μm. Representative of two mice from two experiments.

(C) Representative flow cytometry plot showing (left) APC labeling and (right) surface S1PR1 staining on APC-labeled (i.d. CD45$^+$) and APC-unlabeled (i.d. CD45$^-$) T cells (CD4$^+$CD44$^{lo}$CD69$^-$) in inflamed dLNs. For comparison, surface S1PR1 staining on T cells from blood is also shown for each mouse.

(D) Ratio of S1PR1 mean fluoresence intensity (MFI) on CD45-APC- or CD45-PE-labeled (CD45$^+$) to CD45-APC or CD45-PE unlabeled (CD45$^-$) T cells in dLNs. Each symbol represents one dLN; bars indicate mean. Data are pooled from six $Spns2^{UBC}$ mice and seven littermate controls from three experiments. Statistics, two-tailed unpaired Student's t test.
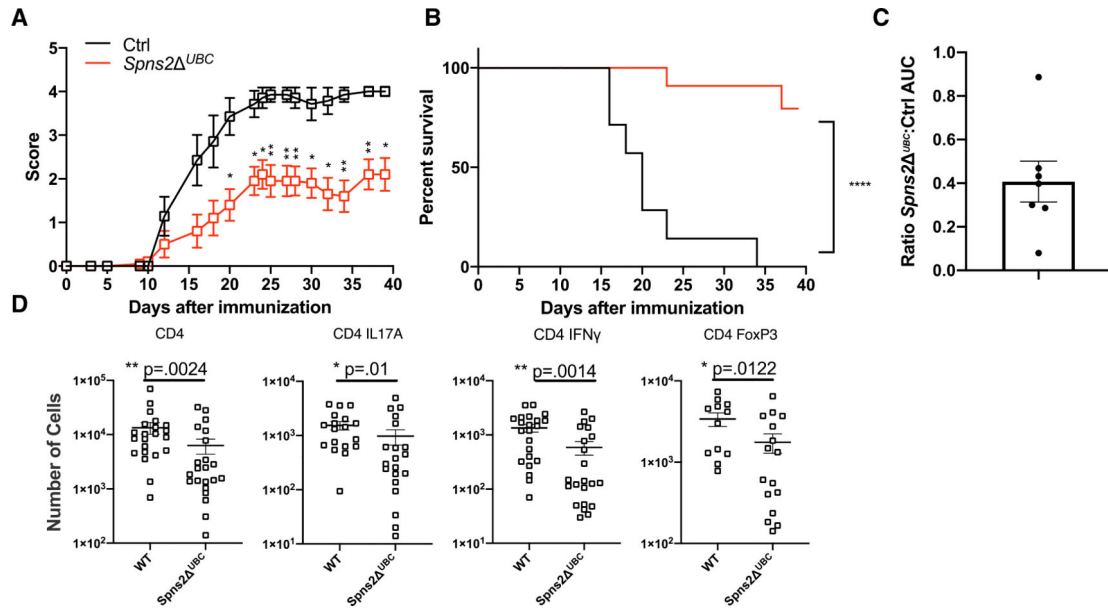
**Figure 4. SPNS2-deficient mice are protected from EAE**

(A and B) 12- to 14-week-old female *Spns2*$^{UBC}$ mice (n = 10) and littermate controls (n = 7) were treated with tamoxifen daily for 5 days. 11 days after the last tamoxifen dose, EAE was induced by myelin oligodendrocyte (MOG)/complete Freund's adjuvant (CFA) immunization. Mice were monitored for clinical signs and euthanized if they maintained a disease score of 4 for 24 h or reached a disease score of 5. (A) Disease scores over time. Day 0 is defined as the day of MOG/CFA injection. Scores from euthanized mice were included as their last score for the remainder of the study. Each symbol represents the mean score ± SEM. *p < 0.05; **p < 0.01 (two-tailed unpaired Student's t test corrected for multiple comparisons by the Holm-Sidak method). (B) Percent of mice that reached humane endpoints over time. ****p < 0.0001 (log rank Mantel-Cox test).

(C) Compilation of seven experiments. The area under the disease curve (AUC) was calculated for control and *Spns2*$^{UBC}$ mice in each of 7 experiments (50 control and 57 *Spns2*$^{UBC}$ mice total). For each experiment, the ratio of the AUC in *Spns2*$^{UBC}$ versus control mice was calculated. Each point represents one experiment; bars represent mean ± SEM.

(D) Enumeration of total CD4 T cells, CD4 T cells producing the cytokines IFN-γ and IL-17A, and CD4 T cells expressing FoxP3 in the central nervous system of control and *Spns2*$^{UBC}$ mice with EAE. Control and *Spns2*$^{UBC}$ mice were co-housed and analyzed when one mouse in the cage reached a score of 2–3. Lymphocytes were isolated from brain and spinal cord; for IFN-γ and IL-17A staining, they were restimulated for 3 h with PMA/ionomycin prior to staining. The sample was split in two (for cytokine and transcription factor staining), the entire sample was analyzed on flow cytometry, and numbers indicate the total number of cells in the indicated gate (CD4 numbers were taken from the restimulated sample). For CD4 and IFN-γ, data compile 10 experiments; for IL-17A, data compile 9 experiments; for FoxP3, data compile 7 experiments. Bars represent mean +/− SEM. See also Figures S1 and S2.

**KEY RESOURCES TABLE**

| REAGENT or RESOURCE | SOURCE | IDENTIFIER |
|---|---|---|
| Antibodies | | |
| CD3ε, PE (clone 145–2C11) | Biolegend | Cat# 100308; RRID: AB_312673 |
| CD4, PerCP (clone RMA 4–5) | Biolegend | Cat# 100537; RRID: AB_893331 |
| CD8, PE-Cy7 (clone 53–6.7) | Biolegend | Cat# 100721; RRID: AB_312760 |
| CD44, AF700 (clone IM7) | Biolegend | Cat# 103025; RRID: AB_493712 |
| B220/CD45RO, PerCP-Cy5.5 (clone RA3– 6B2) | Biolegend | Cat# 103209; RRID: AB_312994 |
| CD69, APC-Cy7 (clone H1.2F3) | Biolegend | Cat# 104526; RRID: AB_10679041 |
| CD62L, BV510 (clone MEL-14) | Biolegend | Cat# 104441; RRID: AB_2561537 |
| Nk-1.1, PerCP-Cy5.5 (clone PK136) | Biolegend | Cat# 108727; RRID: AB_2132706 |
| anti-I-A/I-E, PerCP-Cy5.5 (clone M5/ 114.15.2) | Biolegend | Cat# 107625; RRID: AB_2191072 |
| CD11c, PerCP-Cy5.5 (clone N418) | Biolegend | Cat# 117327; RRID: AB_2129642 |
| CD45.1, APC (clone A20) | Biolegend | Cat# 110714; RRID: AB_313503 |
| CD45.1 FITC (clone A20) | Biolegend | Cat# 110718; RRID: AB_492862 |
| CD45.2, APC (clone 104) | Biolegend | Cat# 109814; RRID: AB_389211 |
| CD45.2, FITC (clone 104) | Biolegend | Cat# 109806; RRID: AB_313443 |
| CD14, PerCP-Cy5.5 (clone Sa14–2) | Biolegend | Cat# 123313; RRID: AB_2074185 |
| IL17A, PE (clone TC11–18H10.1) | Biolegend | Cat# 506903; RRID: AB_315463 |
| IFN-γ, APC (clone XMG1.2) | Biolegend | Cat# 505809; RRID: AB_315403 |
| FOXP3, FITC (clone FJK-16 s) | eBioscience | Cat# 14–5773-82; RRID: AB_467576 |
| LYVE1, FITC (clone ALY7) | eBioscience | Cat# 14–0443-82; RRID: AB_1633414 |
| Mouse S1P$_1$/EDG-1 (clone 713412) | R&D Systems | Cat# MAB7089; RRID: AB_10994183 |
| Biotin-SP (long spacer) AffiniPure F(ab')$_2$ Fragment Donkey Anti-Rat IgG (H+L) | Jackson Immunoresearch | Cat# 712–066-15; RRID: AB_2340653 |
| CD4, BUV395 (clone RM4–5) | BD Biosciences | Cat# 740208; RRID: AB_2734761) |
| mouse TCR Vβ5.1,5.2, PE (clone MR9–4) | Biolegend | Cat# 139504; RRID: AB_10613279 |
| Cd45.2, PE (clone 104) | Biolegend | Cat# 109808; RRID: AB_313445 |
| CD16/32 (clone 93) | Biolegend | Cat# 101302; RRID: AB_312801 |
| CD45, PE (clone 30-F11) | Biolegend | Cat# 147712; RRID: AB_2563598 |
| CD45, APC (clone 30-F11) | Biolegend | Cat# 103112; RRID: AB_312977 |
| Biological samples | | |
| *Mycobacterium tuberculosis* H37Ra, Desiccated | BD Biosciences | Cat# BD 231141 |
| Chemicals, peptides, and recombinant proteins | | |
| Ovalbumin | SigmaAldrich | Cat# A2512 |
| Adjuvant, Incomplete (Freund) | BD Difco | Cat# BD 263910 |
| Fingolimod (FTY720) | Cayman Chemical | Cat# 10006292 |
| MOG 35–55 peptide | Genscript | Cat# RP10245 |
| Pertussis toxin | List Biological Laboratories | Cat# 181 |

| REAGENT or RESOURCE | SOURCE | IDENTIFIER |
|---|---|---|
| Tamoxifen | SigmaAldrich | Cat# T5648 |
| Invitrogen UltraPure Phenol:Chloroform:Isoamyl Alcohol (25:24:1, v/v) | Invitrogen | Cat# 15593031 |
| Sodium Acetate (3 M), pH 5.5, RNase-free | Invitrogen | Cat# AM9740 |
| Percoll | GE Healthcare/Cytiva | Cat# 17089101 |
| SouthernBiotech Fluoromount-G Slide Mounting Medium | Southern Biotech | Cat# 010001 |
| PMA | SigmaAldrich | P8139 |
| GolgiPlug | BD Biosciences | 555029 |
| ionomycin | SigmaAldrich | 19657 |
| Critical commercial assays | | |
| LIVE/DEAD Fixable Blue Dead Cell Stain Kit, for UV excitation | ThermoFisher | Cat# L23105 |
| LightCycler 480 SYBR Green I Master | Roche Diagnostics | Cat# 04707516001 |
| CellTrace Violet Cell Proliferation Kit | ThermoFisher | Cat# C34557 |
| Transcription-Factor Buffer Set | BD PharMingen | Cat# 562574 |
| Deposited data | | |
| Source data | Mendeley Data | https://doi.org/10.17632/2wkphfrn84.2 |
| Experimental models: Organisms/strains | | |
| $Spns2^{f/f}$ | NIH Knockout Mouse Project | EPD0090_5_B04 |
| $Lyve1$-Cre | Pham et al., 2010 | Jackson Laboratories Stock No: 012601 |
| $UBC$-CreERT2 | Ruzankina et al., 2007 | Jackson Laboratories Stock No: 008085 |
| $UBC$-GFP | Schaefer et al., 2001 | Jackson Laboratories Stock No: 004353 |
| OT-II | Barnden et al., 1998 | Jackson Laboratories Stock No: 004194 |
| C57BL/6 | Charles River/ Jackson Laboratories | N/A |
| CD45.1$^+$ C57BL/6 | Charles River/ Jackson Laboratories | N/A |
| Oligonucleotides | | |
| 5′-GACGCTGAGGCATGAGAGCAT-3′ | Barman et al., 2008 | SFB736F |
| 5′-GACGGCACGGATTGTTATTCA-3′, | Barman et al., 2008 | SFB844R |
| 5′- ACTCCTACGGGAGGCAGCAGT-3′ | Amann et al., 1990 | UniF34 |
| 5′- ATTACCGCGGCTGCTGGC-3′ | Amann et al., 1990 | UniR514 |
| Software and algorithms | | |
| FlowJo version 9 | TreeStar | https://www.flowjo.com/solutions/flowjo/downloads |
| GraphPad Prism version 9 | GraphPad | https://www.graphpad.com/scientific-software/prism/ |
| ImageJ v1.49 | NIH | https://imagej.nif.gov/ij/download.ftml |

| REAGENT or RESOURCE | SOURCE | IDENTIFIER |
|---|---|---|
| ZEN 2010 | Zeiss | https://www.zeiss.com/microscopy/us/products/microscope-software/zen.html |
| FACSDiva v8.02 | BD | https://www.bdbiosciences.com/en-us/products/software/instrument-software/bd-facsdiva-software#Overview |
| Other | | |
| Zirconia/silica beads | BioSpec | Cat# 11079101z |
| Beadbeater | Retsch | MM301 |
| LightCycler® 480 System | Roche Diagnostics | 05015243001 |
| LSRII Flow Cytometer | BD | N/A |
| Zeiss 710 inverted confocal microscope | Zeiss | N/A |
| Streptavidin APC | Biolegend | Cat# 405207 |
| Streptavidin PE-Cy7 | Biolegend | Cat# 405206 |
| Medimachine tissue homogenizer system | BD | BD 340588 |
| Beckman Coulter Multisizer 3 | Beckman Coulter | 383601 |